^{209}Bi(^{3}He,d)^{210}Po and ^{209}Bi(^{4}He,t)^{210}Po reactions and some matrix elements of the residual interaction

R. Groleau and W. A. Lanford*
A. W. Wright Nuclear Structure Laboratory, Yale University, New Haven, Connecticut 06520

R. Kouzes
Joseph Henry Laboratories, Princeton University, Princeton, New Jersey 08540

(Received 24 March 1980)

The (^{3}He,d) and (^{4}He,t) single proton transfer reactions on ^{208}Pb and ^{209}Bi were studied using 30 and 40 MeV He beams. The outgoing reaction products were detected by a position sensitive proportional counter in the focal plane of a quadrupole-three-dipole spectrometer. The resolution varied between 10 and 14 keV full width at half maximum. Using the ratio of cross sections for the (^{3}He,d) and (^{4}He,t) reactions to determine l transfers, spectroscopic factors for the reactions on ^{209}Bi have been measured relative to the transitions to the single-particle states observed in reactions on ^{208}Pb. Sum rules are applied and diagonal matrix elements of the effective interaction between valence protons around the ^{208}Pb core are deduced. The matrix elements obtained from empirical interactions and from realistic calculations are compared to these extracted matrix elements.

[NUCLEAR REACTIONS ^{209}Bi(^{3}He,d)^{210}Po, ^{208}Pb(^{3}He,d)^{209}Bi $E_{^{3}\mathrm{He}}$=30 MeV and ^{209}Bi(^{4}He,t)^{210}Po, ^{208}Pb(^{4}He,t)^{209}Bi $E_{^{4}\mathrm{He}}$=40 MeV. Measured differential cross sections with a resolution of 10–14 keV (FWHM). Sum rule analysis and deduction of matrix elements of the residual interaction in nuclei.]

INTRODUCTION

The ^{208}Pb region provides a good region in which to test various nuclear models. Most model calculations assume that the states strongly excited by single proton transfer reactions on ^{208}Pb are pure single particle states and that states in ^{210}Po can be described via a shell model with two valence protons distributed over these single particle orbits. These same assumptions are used in the analysis of the present experiment in order to make as direct a comparison as possible between the theory and experiment. Measurement of the single particle transfer reactions ^{209}Bi(^{4}He, t)^{210}Po and ^{209}Bi(^{3}He, d)^{210}Po relative to the single particle transitions in the ^{208}Pb(^{4}He, t)^{209}Bi and ^{208}Pb(^{3}He, d) ^{209}Bi reactions allows us to determine the relative spectroscopic factors to an accuracy of a few percent, eliminating most of the usual uncertainties associated with the use of the distorted-wave Born approximation (DWBA). This precision allows the useful application of sum rules. Most interestingly, the energy weighted sum rules of Bansal and French[1] can be applied to deduce the diagonal matrix elements of the residual interaction. The high angular momentum of the proton single particle states provides many states over which to study the residual interaction. A simple empirical interaction is deduced which reproduces the general trend of the matrix elements. The empirical Schiffer-True[2] matrix elements and the realistic calculation of Kuo and Herling[3] are also compared to the experimental matrix elements. In this latter case, general qualitative agreement is found, but some important discrepancies also exist.

The three multiplets $|h_{9/2}\otimes h_{9/2}\rangle$, $|h_{9/2}\otimes f_{7/2}\rangle$, and $|h_{9/2}\otimes i_{13/2}\rangle$ of the ^{210}Po spectrum have previously been studied by Lanford *et al.*[4] The present work measures these three multiplets with better resolution and better statistics and in addition measures the $|h_{9/2}\otimes f_{5/2}\rangle$ multiplet and part of the $|h_{9/2}\otimes p_{3/2}\rangle$ multiplet at higher excitation energy.

I. EXPERIMENTAL PROCEDURE

The (^{4}He, t) and (^{3}He, d) reactions on ^{208}Pb and ^{209}Bi were studied using 40 MeV ^{4}He and 30 MeV ^{3}He beams from the Princeton Cyclotron. The target thicknesses ranged from 65 to 160 μg/cm^2 on 5 and 10 μg/cm^2 carbon backings. The lead target was make of 99% isotopically enriched ^{208}Pb and the bismuth target was made of naturally monoisotopic ^{209}Bi.

The beam on target was monitored by measuring the total charge collected in the Faraday cup and by measuring the number of beam particles elastically scattered into a silicon surface-barrier monitor detector at 65°. The relative normalization obtained by the two measurements agreed to within 10%. For the analysis, the elastic scattering data were used to normalize the spectra taken at different angles and different excitation ener-

gies.

To normalize Bi relative to Pb data using the monitor detector, a correction must be made for the different elastic cross sections on Bi and Pb. This was done by requiring that the monopole sum rule, as discussed below, be satisfied for the $h_{9/2}$ orbit. The corrections are 0.93 for ^{3}He beams and 0.88 for ^{4}He, in agreement with calculations of elastic scattering data using DWBA which predicts 0.93 for ^{3}He and 0.91 for ^{4}He.

The tritons and deuterons were detected with a single-wire charge-division position-sensitive proportional counter in the focal plane of the Princeton quadrupole-three dipole (Q-3D) magnetic spectrograph, allowing on-line data acquisition. Dispersion matching of the beam across the target was used to optimize the resolution, which varied between 10 and 14 keV (FWHM).

The (^{4}He,t) spectra were measured at 10° and 20°; the (^{3}He,d) spectra were measured at 20°, 30°, 40°, and 50°. Figure 1 shows the experimental spectra on ^{208}Pb and ^{209}Bi as a function of Q value for the (^{4}He,t) reaction at 20°. Figure 2 gives the (^{3}He,d) spectra at 40°. The single particle levels are labeled in the spectra of reactions on the ^{208}Pb closed core. Various multiplets corresponding to the single particle levels are clearly visible in the spectra of reactions on ^{209}Bi which has an $h_{9/2}$ proton outside the ^{208}Pb closed core. The measured

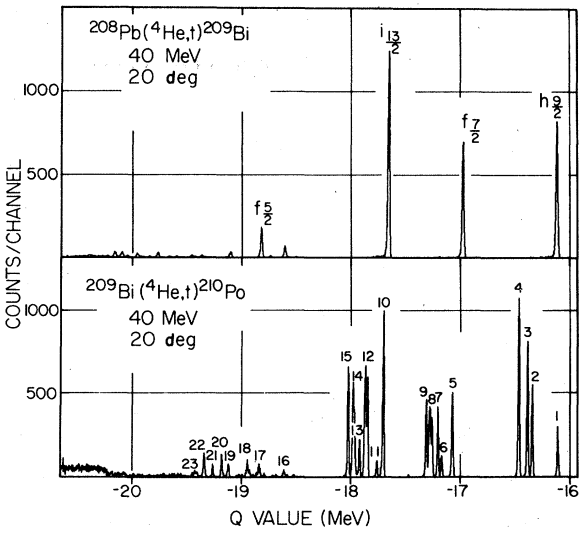

FIG. 1. Experimental spectra of (^{4}He,t) at 40 MeV and 20° on ^{208}Pb and ^{209}Bi. The spectrum on ^{208}Pb displays the single particle levels. The spectrum on ^{209}Bi displays the two particle spectrum obtained by coupling the $h_{9/2}$ ground state proton of the ^{209}Bi target to the proton transferred in one of the single particle levels observed in the spectrum on ^{208}Pb. The (^{4}He,t) reaction favors the cross section to large l-transfer states ($l \sim 5$).

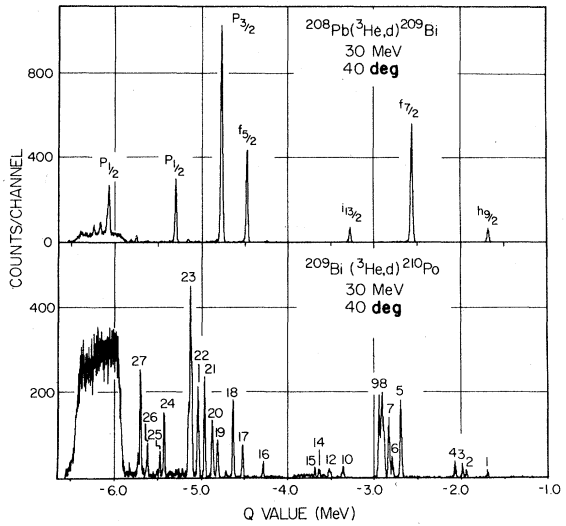

FIG. 2. Experimental spectra of (^{3}He,d) at 30 MeV and 40° on ^{208}Pb and ^{209}Bi. The spectrum on ^{208}Pb displays the single particle levels. The spectrum on ^{209}Bi displays the two particle spectrum obtained by coupling the $h_{9/2}$ ground state proton of the ^{209}Bi target to the proton transferred in one of the single particle levels observed in the spectrum on ^{208}Pb. The (^{3}He,d) reaction favors the cross section to small l-transfers states ($l \sim 0$). The large peak found at −6.2 MeV is caused by a carbon impurity. The peak is broad because the spectrograph is out of focus for the reaction on carbon.

excitation energies of members of the low lying multiplets are compared with levels from the literature in Table I. The excitation energies are accurate to 1 keV per MeV of excitation energy. The measured excitation energies of the single particle levels are given in Table II.

The cross sections to levels not fully resolved were extracted by a peak fitting procedure, using the shape of a nearby single transition peak as reference peak shape. The levels with large cross sections can be extracted unambiguously. Part of the uncertainty in the peak fitting procedure comes from the change in peak shape as a function of position in the focal plane. To minimize this effect, reference peaks were always chosen from among peaks having good statistics and lying close to the multiplet structure of interest. In general, it was found that the high energy sides of the reference peaks had regular Gaussian shapes, while the low energy sides had a small tail, as shown in Fig. 3(a). Because of the poorer statistics of low cross-section levels, the extraction of strengths by peak fitting has more uncertainty for the low spin members of multiplets. The results given in Table I for excitation energies and spectroscopic strengths are the average of the various data.

TABLE I. Spectroscopic factors.

Peak no.	i_j	J^π	$\frac{(2J+1)}{(2J_1+1)}\tilde{C}^2S(\alpha,t)$	$\frac{(2J+1)}{(2J_1+1)}C^2S(^3\mathrm{He},d)$	Weak coupling prediction	Exp. energy (MeV)	Published energy (MeV)	Published J^π
1	$h_{9/2}$	2^+	1.00 ± 0.06	1.16 ± 0.22	1.00	1.181	1.181	2^+
2		4^+	1.79 ± 0.07	1.58 ± 0.28	1.80	1.426	1.427	4^+
3		6^+	2.64 ± 0.09	2.63 ± 0.25	2.60	1.474	1.473	6^+
4		8^+	3.40 ± 0.11	3.42 ± 0.26	3.40	1.557	1.557	8^+
5	$f_{7/2}$	8^+	1.71 ± 0.03	1.64 ± 0.05	1.70	2.188	2.188	8^+
6		2^+	0.416 ± 0.011	0.417 ± 0.02	0.50	2.290	2.290	$(2^+,3^+)$
7		6^+	1.31 ± 0.03	1.26 ± 0.04	1.30	2.325	2.325	6^+
8		1^+	(0.31)	(0.35[a])	0.30	2.391		
		3^+	(0.72)	(0.75[a])	0.70	2.412		
		4^+	(0.90[b])	(0.90[b])	0.90	2.382	2.383	4^+
		5^+	(1.10[b])	(1.10[b])	1.10	2.403	2.403	5^+
		Total[d]	3.08 ± 0.07	3.09 ± 0.10				
9		7^+	1.51 ± 0.03	1.50 ± 0.06	1.50	2.439	2.438	7^+
10(A)						2.872	2.874[c]	
10	$i_{13/2}$	11^-	3.25 ± 0.06		2.30	2.851	2.849	11^-
11		5^-	0.308 ± 0.009		1.10	2.911	2.910	5^-
12		5^-	(0.78)		1.10	3.026	3.026	5^-
		2^-	(0.54)		0.50	3.028		
		7^-	(1.53)		1.50	3.017	3.017	$(7,8)^-$
		9^-	(1.88)		1.90	3.000	~3.009	9^-
		Total[d]	4.85 ± 0.078					
13		4^-	0.782 ± 0.018		0.90	3.079	3.075	(4^-)
14		6^-	(1.34)		1.30	3.125	3.125	$(4,5,6)^-$
		8^-	(1.66)		1.70	3.137	3.138	8^-
		Total[d]	3.13 ± 0.05					
15		10^-	2.11 ± 0.04		2.10	3.185	3.182	10^-
16	$f_{5/2}$	2^+	0.354 ± 0.021		0.50	3.792		
17		4^+	0.60		0.90	4.027		
18		6^+	0.82		1.30	4.139		
19		3^+	0.86 ± 0.04		0.70	4.320		
20		5^+	1.19 ± 0.05		1.10	4.382		
21		6^+	0.55 ± 0.03		1.30	4.469		
22		$7^+,4^+$	1.83 ± 0.07		1.50, 0.90	4.553		
17	$p_{3/2}$, $p_{1/2}$	4^+		0.03		4.027		
18		6^+		0.198	1.30	4.139		
21		6^+		0.557 ± 0.039	1.30	4.469		
22		4^+		0.351 ± 0.07	0.90	4.553		
23		3^+		(0.75)	0.70	4.591		
		(5^+)		(1.35)	1.10	4.624		
		(6^+)		(0.55)	1.30	4.644		
		Total[d]		2.65 ± 0.08				

TABLE I. (*Continued.*)

Peak no.	i_j	J^π	$\frac{(2J+1)}{(2J_1+1)}\tilde{C}^2S(\alpha,t)$	$\frac{(2J+1)}{(2J_1+1)}\tilde{C}^2S(^3\mathrm{He},d)$	Weak coupling prediction	Exp. energy (MeV)	Published energy (MeV)	Published J^π
24			0.336 ± 0.02		4.991			
25			0.123 ± 0.012		5.041			
26			0.189 ± 0.015		5.186			
27			0.652 ± 0.033		5.270			

[a] Poor statistics.
[b] These levels are well known from γ ray work and their full strength is assumed in the peak fitting.
[c] Reference 15.
[d] The numbers in parentheses result from unfolding an unresolved multiplet using a peak fitting procedure. The totals given are the integrated strengths for these multiplets and are more accurate than individual strengths.

Examples of peak fitting are shown in Fig. 3 for multiplets for which peak fitting was required. These fits are discussed in detail below.

II. ANALYSIS

Because of their large Q-value differences, the (^{4}He,t) and (^{3}He,d) reactions favor different angular momentum transfers. The −14.837 MeV ground state Q-value for the (^{4}He,t) reaction has an angular momentum matching at $l \simeq 5$, while the −0.516 MeV ground state Q value for the (^{3}He,d) reaction has an angular momentum matching at $l \simeq 0$. As a result, the ratio of cross sections for these two reactions to a particular final state is a strong function of the angular momentum transferred to that individual state. The Q-value dependence of this ratio has been calculated with DWBA using the code DWUCK .[5]

This procedure of using the cross-section ratio $R(l) = \sigma(^{3}\mathrm{He},d)/\sigma(^{4}\mathrm{He},t)$ to determine the angular momentum transfers has a number of advantages over the more conventional method of measuring complete angular distributions. In addition to being unambiguous and very efficient, it allows the simultaneous study of states excited via both low and high l-transfer values. For example, comparison between Figs. 1 and 2 shows that the (^{4}He,t) reaction cross section is large for states formed with $l=5$ and $l=6$, while the (^{3}He,d) reaction cross section is large for $l=1$ states.

The optical model potential parameters used in DWUCK are shown in Table III. For the (^{4}He,t) reaction, the parameters from Lilley and Stein[6] were used. The parameters give a good fit to the detailed angular distributions obtained from ^{208}Pb (^{4}He,t)^{209}Bi at 42 MeV. For the (^{3}He,d) reaction, the parameters are from Wildenthal *et al.*[7] They give a good fit to our limited angular measurements.

The experimental ratios $R(l)[=\sigma(^{3}\mathrm{He},d)/\sigma(^{4}\mathrm{He},t)]$ of the cross sections for the two reactions are shown in Figs. 4(a) and 4(b). The error bars reflect statistical uncertainty only and are given only when larger than the plotted data point. In both figures, the ratios are those between (^{3}He,d) data measured at 40° and (^{4}He,t) data measured at 20°. These measured cross sections are given in Table IV. Similar analyses of the data at other angles is in agreement with the results in these two figures.

The experimental ratios of the cross sections for the two reactions leading to states in ^{209}Bi are shown in Fig. 4(a). The lines have been calculated with DWUCK for various Q values and for each l transfer. For $l=1, 3$, and 6, there are two experimentally observed single particle levels having the same l value and which are well known from

TABLE II. Spectroscopic factors in ^{209}Bi.

Orbit	Exc. energy (MeV)	Pub. energy (MeV)	Spectroscopic factors (^{4}He, t) Present experiment	(^{4}He, t) From Ref. 6	(^{3}He, d) Present experiment	(^{3}He, d) From Ref. 6	(^{3}He, d) From Ref. 7
$h_{9/2}$	0.000	0.000	1.0 [a]	1.0 [a]	1.0 [a]	0.95	1.0 [a]
$f_{7/2}$	0.899	0.897	0.89	1.04	1.38	1.18	1.12
$i_{13/2}$	1.613	1.608	1.05	1.01	0.85	0.88	0.94
$i_{13/2}$	2.601	2.599	0.09	0.09	0.08		
$f_{5/2}$	2.826	2.826	0.65	0.91	0.87	1.15	1.14
$p_{3/2}$	3.121	3.118			0.98	1.03	1.08
$p_{1/2}$	3.635	3.633			0.54	0.63	(0.7–0.9)

[a] The calculation was normalized assuming $C^2S = 1.0$ for this state.

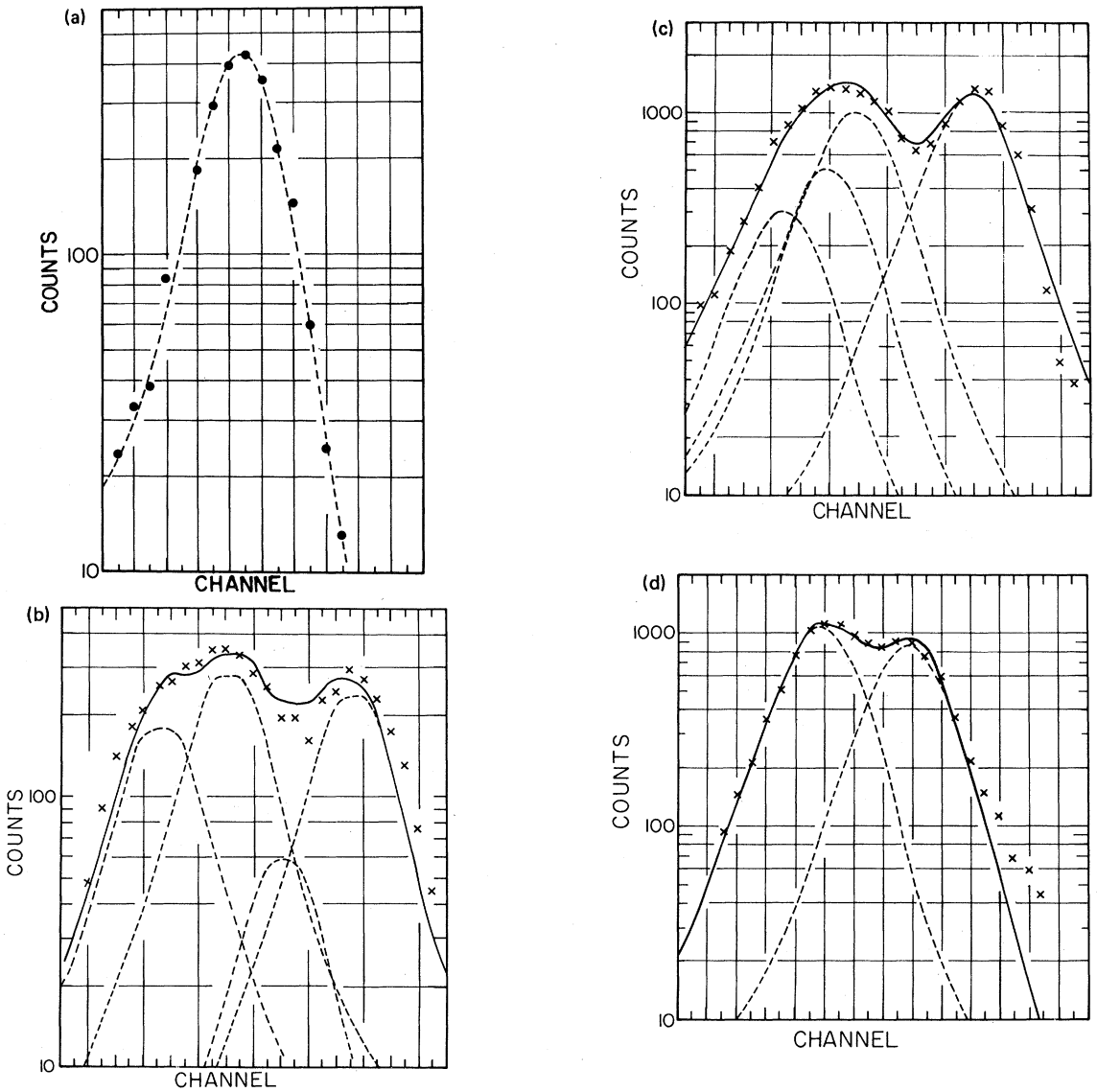

FIG. 3. (a) Typical reference peak used in the peak fitting procedure. The high energy side of the peak has a regular Gaussian shape, while the low energy side has a small tail. (b) Typical fits obtained for the group of levels at 2.4 MeV of excitation energy in the $|h_{9/2} \otimes f_{7/2}\rangle$ configuration. (c) Typical fits obtained for the group of levels at 3.0 MeV of excitation energy in the $|h_{9/2} \otimes i_{13/2}\rangle$ configuration. (d) Typical fits obtained for the group of levels at 3.13 MeV of excitation energy in the $|h_{9/2} \otimes i_{13/2}\rangle$ configuration.

TABLE III. DWUCK optical potential parameters.

	V_0 (MeV)	W_0 (MeV)	r_0 (fm)	r_{0c} (fm)	a (fm)	r' (fm)	a' (fm)	W_0' (MeV)	λ
(^{4}He,t) [a]									
t	−200	−50	1.45	1.30	0.60	1.45	0.60		
^{4}He	−200	−20	1.40	1.30	0.60	1.40	0.60		
p			1.24	1.20	0.65				0.0
(^{3}He,d) [b]									
d	−111		1.05	1.25	0.859	1.24	0.794	70.8	
^{3}He	−175	−17.5	1.14	1.40	0.723	1.60	0.81		
p			1.24	1.25	0.65				6.0

[a] From Ref. 6.
[b] From Ref. 7.

previous experiments.[6,7] As shown in Fig. 4(a), the calculated $R(l)$ have the correct energy dependence to reproduce the experimental ratios for these three cases, thus confirming that the Q-value dependence of these reactions is predicted accurately by DWBA.

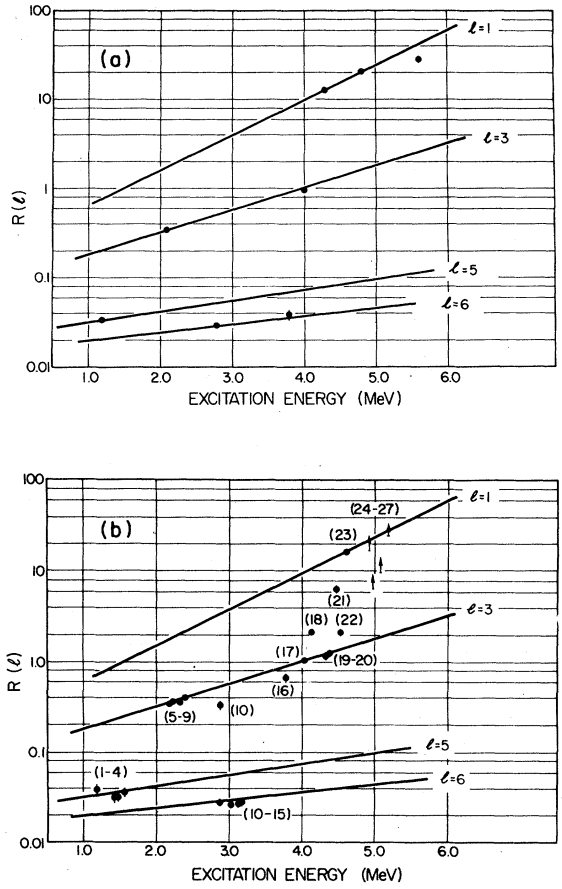

FIG. 4. Experimental ratios $R(l)$. $R(l)$ is the ratio of the cross sections for (^{3}He,d) at 40° to the cross section for (^{4}He,t) at 20°. The excitation energies are given relative to the ground state of ^{210}Po. The error bars are due to statistical uncertainties and are given only when larger than the plotted data point. (a) $R(l)$ for the ^{209}Bi spectrum. (b) $R(l)$ for the ^{210}Po spectrum.

The experimental ratios of the cross sections, $R(l)$, for the states in ^{210}Po are shown in Fig. 4(b). The lines are the same as those in Fig. 4(a). Deviation from a line in this display indicates an l admixture. As shown in Fig. 4(b), the low lying multiplets excited via $h_{9/2}$, $f_{7/2}$, and $i_{13/2}$ transfers lie, within experimental uncertainties, on pure $l=5$, $l=3$, and $l=6$ lines, respectively.

In the region above 3 MeV of excitation, three states are excited by pure $l=3$ transitions. We interpret these as members of the $h_{9/2}\otimes f_{5/2}$ multiplet. In addition, four states correspond to points off the $l=3$ line as shown in Fig. 4(b). The levels at 4.133, 4.460, and 4.538 MeV are excited with ratios $R(l)$ falling between the pure $l=1$ and $l=3$ lines, indicating an admixture of these two angular momenta. An $l=1$ and $l=5$ admixture for such strong states is eliminated because of the intrinsically small $l=5$ cross section for the (^{3}He,d) reaction. The level at 3.787 MeV corresponds to a point slightly below the $l=3$ line. Admixture with l larger than 3 or accidental degeneracy could explain this.

A. ^{209}Bi spectroscopic factors

For the purpose of our analysis, the six levels strongly excited in the ^{208}Pb(^{3}He,d)^{209}Bi and ^{208}Pb (^{4}He,d)^{209}Bi reactions are assumed to be pure single particle shell model levels. In fact, the measurements of the cross sections on the ^{208}Pb target were made to determine the unit strengths (cross sections) for transfer to these single particle orbits. These experimentally measured unit strengths will be used below in the analyses of the reactions on a ^{209}Bi target. However, first we examine how valid the assumption of the purity of the levels appears to be.

A measure of the purity of the single particle levels is given by the absolute spectroscopic factors C^2S. In the conventional DWBA theory applied

TABLE IV. Absolute cross sections in ^{210}Po.

Peak no.[a]	Cross sections (μb/sr)[b] $(^4\text{He},t)_{20°}$	$(^3\text{He},d)_{40°}$
1	190	7
2	330	10
3	498	16
4	612	23
5	350	120
6	82	30
7	256	91
8 + 9	889	360
9	287	
10(A)	22	7
10	546	15
11	50	2
12	834	22
13	126	9
14	526	14
15	352	10
16	27[c]	2
17	46[c]	49
18	52[c]	110
19	53	62
20	77	97
21	35	190
22	108	230
23	42	690
24	<5	88
25	<5	32
26	<5	49
27	<7	170

[a] The peak numbers correspond to the peak numbers of the spectra shown in Figs. 1 and 2.

[b] The cross sections are accurate to about 15%.

[c] Extraction of the cross section limited by background uncertainty.

to a spin zero target, the proton stripping cross section is given by

$$\sigma_{\text{exp}}(\theta) = N(C^2S)\sigma_{\text{DW}}(\theta)\text{fm}^2/\text{sr}\,, \tag{1.1}$$

where $\sigma_{\text{DW}}(\theta)$ is the distorted wave cross section and N is a normalization factor which can be calculated only approximately, but which is constant for a given reaction. By choosing N so that the $h_{9/2}$ transition has unit strength, expression (1.1) can be used to deduce spectroscopic factors for transitions with other l_j values in ^{209}Bi.

The results of the present measurements are compared with other values from the literature in Table II. As shown in this table, the spectroscopic factors are close to unity, indicating the purity of the levels. A notable exception is the $p_{1/2}$ level at 3.637 MeV which has a spectroscopic factor of order 0.5; another $p_{1/2}$ level at 4.421 MeV contains most of the rest of the strength. In general, our spectroscopic factors agree well with those obtained by others.

The proton single particle orbits in ^{209}Bi are represented in the usual shell model by the wave functions $|l_j \otimes ^{208}\text{Pb}(0^+)\rangle$. These wave functions can be used to evaluate the expectation values for the electric quadrupole and magnetic dipole moment operators. To reproduce the experimental values of these electromagnetic moments, the valence nucleon has to take an effective charge and an effective magnetic dipole moment significantly different from those of a free proton.[8] This "renormalization" of the moments is caused by the polarization of the ^{208}Pb core induced by the valence proton. As indicated by the moments, this induced polarization is substantial and the valence nucleon wave functions $|l_j \otimes ^{208}\text{Pb}(0^+)\rangle$ represent "quasiprotons", i.e., valence protons with the appropriate charges and magnetic moments. Study of the spectra of 3 or more valence nucleons outside the ^{208}Pb core and the electromagnetic moments for nuclei with 2 or more valence nucleons suggest that the core polarization associated with a valence nucleon is to a large extent independent of the presence of other valence nucleons.[9,10] The effective interaction discussed below is the interaction between these valence protons with their associated core polarizations.

B. ^{210}Po spectroscopic factors

Because ^{209}Bi has an $h_{9/2}$ proton outside the ^{208}Pb closed core, it is expected that in the reaction on a ^{209}Bi target the single particle transitions l_j observed in the proton transfer reaction on ^{208}Pb will be split into multiplets with configuration of $|h_{9/2} \otimes l_j\rangle$.

Using the reaction on ^{208}Pb to obtain the unit cross sections for the single particle transitions, the relative spectroscopic factors ($\tilde{C}^2S$) can be extracted from the data using

$$\sigma_{\text{exp}}^{\beta,J}(\theta) = \sum_{l_j} \frac{(2J+1)}{(2J_i+1)} \tilde{C}^2S(\beta, l_j) \frac{\sigma_{l_j}(\theta)}{(2J+1)}, \tag{2.1}$$

where $\sigma_{\text{exp}}^{\beta,J}(\theta)$ is the measured cross section in the ^{210}Po spectra for the level β; J_i is the spin of the target nucleus; J is the spin of the final nucleus; $\tilde{C}^2S(\beta, l_j)$ is the relative spectroscopic factor for the level β of a given l_j and J. The sum is over all possible angular momentum transfers l_j that contribute to the cross section $\sigma_{\text{exp}}^{\beta,J}(\theta)$; $\sigma_{l_j}(\theta)$ is the experimental cross section to the single particle level l_j in ^{209}Bi.

Because transitions to states in ^{210}Pb generally

occur at different Q values than do the transitions to the corresponding single particle states in ^{209}Bi, the experimental cross sections in the ^{210}Po must be corrected for this Q-value difference. These corrections were calculated using DWUCK. Since the Q-value differences between the two reactions are small and since the bombarding energies were high, the corrections are generally only a few percent and it is to be expected that DWUCK should predict these corrections accurately. The good agreement shown in Fig. 4 between the energy dependence calculated using DWUCK and experiment confirms this expectation.

Table I gives the relative spectroscopic strengths $(2J+1)/(2J_i+1)\tilde{C}^2S$ for the various levels excited. The uncertainties quoted are statistical. The spectroscopic strengths in parentheses have been extracted by peak fitting. The energies measured in this experiment are also compared with previous data whenever available.

C. Sum rules

1. The monopole sum rule

For a stripping reaction, the spectroscopic strengths obey the monopole sum rule as given in Ref. 11:

$$\sum_{\substack{\beta,\text{ with } l_j,\\ T \text{ constant}}} \frac{(2J+1)}{(2J_i+1)}\,\tilde{C}^2S(\beta,l_j)=p_j^h-\frac{n_j^h}{(2T_i+1)},$$

where p_j^h and n_j^h are the number of proton and neutron holes, respectively, in orbit l_j; T_i is the isospin of the target. The single particle levels involved in the present experiment are all filled with neutrons, so $n_j^h=0$. The sum rule becomes

$$\sum_{\substack{\beta,\text{ with } l_j\\ \text{constant}}} \frac{(2J+1)}{(2J_i+1)}\,\tilde{C}^2S(\beta,l_j)=p_j^h.$$

Using the spectroscopic strengths from Table I, the experimental sum is compared with the sum rule limit in Table V.

For the $h_{9/2}$ orbit, the number of proton holes is expected to be nine because of the presence of a proton in the ground state of the ^{209}Bi target. Since we did not attempt to measure the cross section to the 0^+ ground state of ^{210}Po, the expected value for the sum rule of the observed $h_{9/2}$ levels becomes 8.8. This sum rule was used to determine the cross sections for reactions on ^{209}Bi relative to reactions on ^{208}Pb. This normalization procedure was checked against the monitor detector and when corrections were made for differences in elastic scattering from ^{209}Bi and ^{208}Pb, these two procedures agree to a few percent as discussed above (see Sec. I).

TABLE V. Monopole sum rule for the (^{4}He,t) and (^{3}He,d) reactions on ^{209}Bi.

Orbit	(^{4}He,t)	(^{3}He,d)	Sum rule limit
$h_{9/2}$	8.80	8.80	8.80
$f_{7/2}$	8.03	7.91	8.00
$i_{13/2}$	14.43		14.0
$f_{5/2}$	6.21		6.0
$p_{3/2}, p_{1/2}$		5.09	6.0

As shown in Table V, the sum rule for $h_{9/2}$, $f_{7/2}$, and $i_{13/2}$ is satisfied within statistical uncertainty. As shown from Fig. 4(b), the $f_{5/2}$ multiplet appears to be mixed with the $p_{3/2}$ and $p_{1/2}$ multiplets. Because of the very low cross section for $l=1$ states in the reaction (^{4}He,t), the high excitation energy multiplet in ^{209}Bi(^{4}He,t)^{210}Po represents essentially only the $f_{5/2}$ transitions. This allows us to deduce the sum of the $f_{5/2}$ spectroscopic strengths in Table V. Subtracting this $f_{5/2}$ contribution from the cross section to the mixed l states in the (^{3}He,d) reaction gives the $l=1$ strength associated with the $p_{3/2}$ and $p_{1/2}$ multiplets. The measured strength is 5.12 compared to the theoretical limit of 6.0. Because the $p_{1/2}$ single particle state in ^{209}Bi is fragmented into two components at 3.637 and 4.421 MeV, some $l=1$ strength in ^{210}Po may be at higher excitation energy than the region studied.

2. The dipole sum rule

A second sum rule can be used to test the data and our analysis. A short discussion following Ref. 12 will be given for stripping reactions. We let $|\alpha J^\pi\rangle$ be a complete set of shell model basis states representing the target nucleus plus the stripped nucleon; we let $|\beta J^\pi\rangle$ be the complete set of physical states. One can expand $|\beta J^\pi\rangle$ as

$$|\beta J^\pi\rangle=\sum_\alpha \langle\alpha|\beta\rangle|\alpha J^\pi\rangle.$$

The spectroscopic factor for the shell model state $|\alpha J^\pi\rangle$ in the physical state $|\beta J^\pi\rangle$ is $|\langle\alpha|\beta\rangle|^2$ and since $|\alpha J^\pi\rangle$ and $|\beta J^\pi\rangle$ are two complete set of states, one can also write

$$|\alpha J^\pi\rangle=\sum_\beta \langle\beta|\alpha\rangle|\beta J^\pi\rangle.$$

Using the orthonormality of the states, one finds

$$\sum_{\substack{\beta\\ \text{fixed } \alpha \text{ and } J^\pi}} \tilde{C}^2S(\beta,l_j)=\sum_{\substack{\beta\\ \text{fixed } \alpha \text{ and } J^\pi}} |\langle\beta|\alpha\rangle|^2=1,$$

where l_j represents the set of shell model states. In terms of the spectroscopic strengths, one has

$$\sum_{\substack{\beta \\ \text{fixed} l_j \text{and} J^\pi}} \frac{(2J+1)}{(2J_i+1)} \tilde{C}^2 S(\beta, l_j) = \frac{(2J+1)}{(2J_i+1)},$$

where $\tilde{C}^2 S(\beta, l_j)$ is the relative spectroscopic factor for state β of angular momentum J formed from the single particle level l_j. J_i is the spin of the target. Using this sum rule and the results of some gamma radiation work,[13] we suggest spins and parities for various levels. The suggested J^π are presented in Table I. These suggestions are discussed in detail below.

III. ANALYSES OF INDIVIDUAL MULTIPLETS

A. $|h_{9/2} \otimes h_{9/2}\rangle$

For $J^\pi = 2^+$, 4^+, 6^+, and 8^+, a single transition exhausts the dipole sum rule strength to within a few percent. This implies that the low lying 2^+, 4^+, 6^+, and 8^+ states are essentially pure $|h_{9/2} \otimes h_{9/2}\rangle$ configuration.

B. $|h_{9/2} \otimes f_{7/2}\rangle$

The 2^+, 6^+, 7^+, and 8^+ states are well resolved single transitions and, except (possibly) for the 2^+ level, the measured strengths agree well with the expected $(2J+1)$ dependence of the dipole sum rule. Spin suggestions based on transfer strength for these levels are in agreement with the gamma radiation work and with other previous measurements. The level at 2.290 MeV has a strength about 20% lower than the sum rule strength for 2^+. From gamma radiation work, the suggested spins are 2^+ and 3^+. We prefer the 2^+ assignment rather than the 3^+ because we have found a state at 2.412 MeV which has the strength expected for a 3^+ state.

The group of states located at about 2.4 MeV was analyzed by peak fitting. Typical fits are shown in Fig. 3(b). The 4^+ and 5^+ assignments are well established from gamma radiation work. Subtracting these peaks, a peak with a strength of 0.72 remains, consistent with a 3^+ assignment. There also consistently appears a small peak of irregular shape with a spectroscopic factor consistent with that of the 1^+ member of this multiplet. The irregular shape probably results from the usual difficulty experienced in extracting weak transitions in the presence of strong ones using the peak fitting procedure.

C. $|h_{9/2} \otimes i_{13/2}\rangle$

The 10^- state at 3.185 MeV is well resolved and has the expected sum rule strength. The level at 2.915 MeV is the low energy part of the split 5^- strength, well established from gamma radiation work. In the weak coupling model of Hamamoto,[14] the mixing occurs between the single particle level $|h_{9/2} \otimes i_{13/2}\rangle_{5^-}$ and the core excited level $|h_{9/2}{}^2 \otimes {}^{208}\text{Pb}(3^-)\rangle_{5^-}$. The strength of the single particle component at 2.915 MeV measured in the present experiment (0.31) is in agreement with the gamma radiation work[13] (0.31).

At about 3.0 MeV, the group of states shown in Fig. 3(c) is observed. A single peak gives a good fit on the low energy side; the strength corresponds to a 9^- state. A 5^- state is known from gamma radiation work to lie at 3.026 MeV. Assuming this state contains the strength missing from the 5^- at 2.915 MeV, we subtracted the 5^- and 9^- contributions from this group of states. The remaining spectrum was well fitted by assuming a strong state at 3.017 MeV (consistent with the strength of the 7^- member of this multiplet), leaving a small peak of irregular shape. The spectroscopic strength of this peak is 0.54, suggesting that it corresponds to the 2^- member of this multiplet. Table I compares our spin suggestions with the gamma radiation work; no discrepancies are found. At 3.130 MeV, the group of states shown in Fig. 3(d) is observed. This multiplet is well fitted by assuming two states with spectroscopic strengths of 1.34 and 1.66 suggesting the 6^- and 8^- assignments, respectively. The level at 3.079 MeV is well resolved. A spin and parity of 4^- is suggested, although the strength is about 10% lower than the sum rule limit for a 4^- state.

The state at 2.581 MeV is too strong to be a pure 11^- state. We believe that the 11^- state lies unresolved with the 3^- state, the only other missing member of the multiplet. Still, the extra strength of the level is not fully understood. This peak consistently had a shoulder with an $R(l)$ below the $l=3$ line, as shown in Fig. 4(b). This transition is probably an $l=3$ and/or $l=5$ transfer to an unidentified level. A state at this energy appears to have been seen in inelastic scattering.[15]

D. $|h_{9/2} \otimes f_{5/2}\rangle$

This multiplet lies close to the $|h_{9/2} \otimes p_{3/2}\rangle$ and $|h_{9/2} \otimes p_{1/2}\rangle$ multiplets, favoring mixing. Because the $l=1$ cross section for the $(^4\text{He}, t)$ reaction is negligible as shown in Fig. 1, the $|h_{9/2} \otimes f_{5/2}\rangle$ component of each level is observed directly in the $(^4\text{He}, t)$ reaction. The spectroscopic strengths given in Table I have been extracted from the $(^4\text{He}, t)$ data.

Figure 4(b) indicates that peaks 17, 19, and 20 correspond to pure $l=3$ transitions while peaks 18, 21, and 22 correspond to transitions having $l=1$

admixtures.

A group of low cross section peaks, appearing only in the (^{4}He,t) reaction, lies in the region of peak 16. The corresponding levels are believed to constitute the multiplet associated with the level at 2.601 MeV excited via $l=6$ in the ^{208}Pb(^{4}He,t)^{209}Bi reaction. This level has been suggested[14] to be an admixture between the $i_{13/2}$ single particle level and the core excited state $|h_{9/2}\otimes^{208}\mathrm{Pb}(3^-)\rangle_{13/2^-}$. It seems plausible that, with the present resolution, an $l=6$ populated level may be unresolved from peak 16, explaining why this peak yields an $R(l)$ which falls below the pure $l=3$ line in Fig. 4(b).

The spin and parity suggestions for this multiplet are based on an assumed $(2J+1)$ dependence of the cross sections and the cross section systematics observed in the other multiplets. A further justification of these suggestions is presented in Appendix A.

E. $|h_{9/2}\otimes p_{3/2}\rangle$ and $|h_{9/2}\otimes p_{1/2}\rangle$

Knowing the spectroscopic strengths of the $l=3$ components of peaks 16 to 22 from the (^{4}He,t) spectrum, we extracted the $l=1$ component from the (^{3}He,d) reaction by subtracting the $f_{5/2}$ contribution from the measured cross section.

The $R(l)$ corresponding to peak 23 lies on the $l=1$ line. The large apparent spectroscopic strength for this peak suggests that it corresponds to an unresolved structure. The strengths deduced using peak fitting are given in Table I. Transitions corresponding to peaks 24, 25, 26, and 27 were not observed in the (^{4}He,t) spectrum. A lower limit for $R(l)$ is given in Fig. 4(b). Transitions corresponding to peaks 24 and 27 lie close to the $l=1$ line. The lower limits for $R(l)$ associated with peaks 25 and 26 lie between the $l=1$ and $l=3$ lines. The spectroscopic strengths extracted for these two latter peaks assume a pure $l=1$ level.

Our spin and parity suggestion are discussed in Appendix A, together with those of the $|h_{9/2}\otimes f_{5/2}\rangle$ multiplet.

IV. DIAGONAL MATRIX ELEMENTS

In the shell model, one assumes that the interaction of a valence nucleon with the core can be described by an average potential. The interaction between two or more valence nucleons is assumed to be small enough to be treated by perturbation theory.

Inasmuch as ^{208}Pb has been shown experimentally to be a closed-core nucleus, the spectrum of ^{210}Po depends directly on the residual interaction between the two valence protons. First order perturbation theory will give the spectrum shown in Fig. 5. From this figure, one could, in principle, extract diagonal matrix elements of the residual interaction.

To extract the matrix elements independent of perturbation theory, we used the energy-weighted sum rule developed by Bansal and French.[1] We let $|\alpha J^\pi\rangle$ be the complete set of orthonormal basis states from the shell model and $|\beta J^\pi\rangle$ be the complete set of orthonormal physical states. One can

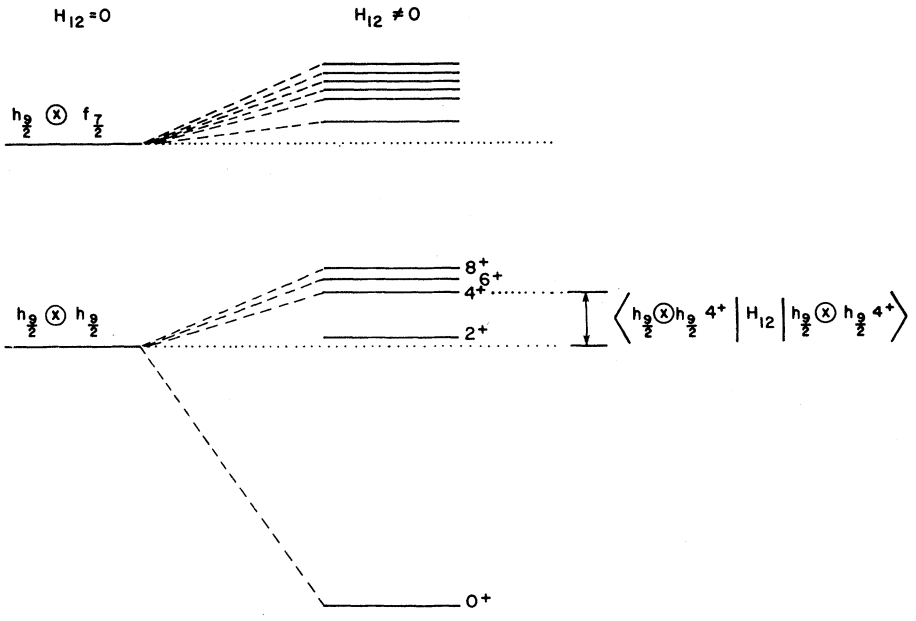

FIG. 5. General splitting of a spectrum (degenerate in zeroth order) by first order perturbation theory.

expand $|\beta J^\pi\rangle$ in terms of the shell model basis:

$$|\beta J^\pi\rangle = \sum_\alpha \langle\alpha|\beta\rangle |\alpha J^\pi\rangle .$$

The two bases being complete, one can use the unitarity of the coefficients $\langle\alpha|\beta\rangle$ to expand $|\alpha J^\pi\rangle$ in terms of the physical states:

$$|\alpha J^\pi\rangle = \sum_\beta \langle\beta|\alpha\rangle |\beta J^\pi\rangle .$$

We let H be the Hamiltonian of the system, such that $H|\beta J^\pi\rangle = E_\beta(J^\pi)|\beta J^\pi\rangle$. We can obtain the diagonal matrix elements of H in the basis $|\alpha J^\pi\rangle$:

$$\langle\alpha J^\pi|H|\alpha J^\pi\rangle = \sum_\beta |\langle\beta|\alpha\rangle|^2 E_\beta(J^\pi),$$

where $|\langle\beta|\alpha\rangle|^2$ is the relative spectroscopic factor $\tilde{C}^2S(\beta, l_j)$. Therefore, we get the expression

$$\langle\alpha J^\pi|H|\alpha J^\pi\rangle = \sum_\beta \tilde{C}^2S(\beta, l_j)E_\beta(J^\pi).$$

This expression can be used to extract the matrix elements of H in a shell model basis. H being the total Hamiltonian, we divide it into three terms: $H = H_{\rm sm} + V_c + V_R$, where $H_{\rm sm}$ is the single particle shell model Hamiltonian, V_c is the Coulomb interaction between the two protons and V_R is the residual interaction. The matrix element $\langle\alpha J^\pi|H_{\rm sm}|\alpha J^\pi\rangle$ gives the single particle energy for each orbit l_j, which is known experimentally from the ^{209}Bi spectrum. The matrix element $\langle\alpha J^\pi|V_R|\alpha J^\pi\rangle$ can be calculated. Hence, we have the expression

$$\langle\alpha J^\pi|V_R|\alpha J^\pi\rangle = \sum_\beta \tilde{C}^2S(\beta, l_j)E_\beta(J^\pi) - \langle\alpha J^\pi|H_{\rm sm}|\alpha J^\pi\rangle - \langle\alpha J^\pi|V_c|\alpha J^\pi\rangle .$$

The Coulomb matrix elements were evaluated in a harmonic oscillator basis, with $\nu = 0.078$ fm^{-2} obtained from electron scattering data. Using the spectroscopic strength of Table I, we evaluated from the above expression the diagonal matrix

TABLE VI. Experimental matrix elements.

Configuration	J^π	Excitation energy (MeV)	Single particle energy (MeV)	Calculated Coulomb matrix element (keV)	Nuclear matrix element (keV)
$h_{9/2}\otimes h_{9/2}$	0^+	0.000	1.175	272	−1.447
	2^+	1.181		234	−228
	4^+	1.426		210	41
	6^+	1.474		199	100
	8^+	1.557		201	181
$f_{7/2}\otimes h_{9/2}$	1^+	2.391	2.073	237	81
	2^+	2.290		225	−8
	3^+	2.412		211	128
	4^+	2.382		205	104
	5^+	2.403		198	132
	6^+	2.325		199	53
	7^+	2.439		198	168
	8^+	2.188		224	−109
$i_{13/2}\otimes h_{9/2}$	2^-	3.028	2.787	242	−1
	3^-	2.851		225	−161
	4^-	3.079		210	82
	5^-	(2.911, 3.028)		204	4
	6^-	3.125		195	143
	7^-	3.017		194	36
	8^-	3.137		189	161
	9^-	3.000		195	18
	10^-	3.185		194	204
	11^-	2.851		228	−164
$f_{5/2}\otimes h_{9/2}$	2^+	3.792	3.999	238	−445
	3^+	4.320		210	111
	4^+	(4.027, 4.553)		207	8
	5^+	4.382		195	188
	6^+	(4.139, 4.469)		202	70
	7^+	4.553		208	346
$p_{3/2}\otimes h_{9/2}$	3^+	4.591	4.291	218	82
	4^+	(4.553)		202	
	(5^+)	4.624		195	138
	6^+	(4.139, 4.469, 4.644)		216	−14

elements of the residual interaction. These matrix elements are given in Table VI.

V. DISCUSSION

The matrix elements of the residual interaction deduced from ^{210}Po describe the interaction between two protons outside the ^{208}Pb core. Hence, in expressing these $T=1$ matrix elements in terms of some empirical potential (V_R), both direct and exchange integrals are needed:

$$\langle j_1 j_2 JT=1 \,|V_R|\, j_1 j_2 JT=1\rangle = J_{12} - (-1)^{j_1+j_2-J} K_{12},$$

where J_{12} = direct integral = $\langle \varphi_{j_1}(1)\varphi_{j_2}(2) V_R \varphi_{j_1}(1)\varphi_{j_2}(2)\rangle$ and K_{12} = exchange integral = $\langle \varphi_{j_1}(1)\varphi_{j_2}(2) V_R \varphi_{j_2}(1)\varphi_{j_1}(2)\rangle$.

The experimental matrix elements of V_R are displayed (vs. J) in Fig. 6 where lines simply connect the data points. The odd and even J's are treated separately because of their different behavior for a short-range interaction. For the $|h_{9/2}\otimes f_{7/2}\rangle$, $|h_{9/2}\otimes i_{13/2}\rangle$, $|h_{9/2}\otimes f_{5/2}$, and $|h_{9/2}\otimes p_{3/2}\rangle$ configurations, most of the matrix elements are repulsive (positive). Note, this is not simply a result of the Coulomb repulsion since these are matrix elements of V_R only, the Coulomb matrix elements having been subtracted.

We tried to reproduce these experimental matrix elements with a simple residual interaction of a pure Wigner type. The matrix elements were calculated with harmonic oscillator wave functions of frequency $\nu = 0.078$ fm^{-2} obtained from electron scattering data and with a Gaussian interaction of variable range and strength. The J dependence of the experimental matrix elements is reproduced well by a short-range (0.82 fm) attractive interaction. However, in order to make these matrix elements positive, a relatively structureless (i.e., almost independent of J) long-range (8.2 fm) repulsive interaction has to be added to the short-range part. The matrix elements of the interaction

$$V_I = -200e^{-(r/0.82)^2} + 0.51e^{-(r/8.2)^2}\ (\text{MeV}),$$

shown in Fig. 7, reproduce the trend of the data well, with a standard deviation of 80 keV.

The standard deviation per degree of freedom was not improved by adding a spin-spin interaction of the form

$$\vec{\sigma}_1\cdot\vec{\sigma}_2 V_0 e^{-(r/r_0)^2}$$

or a short-range (0.82 fm) tensor interaction of the form

$$V_t = V_0 e^{-(r/r_0)^2}(r^{-2})[3(\vec{\sigma}_1\cdot\vec{r})(\vec{\sigma}_2\cdot\vec{r}) - (\vec{\sigma}_1\cdot\vec{\sigma}_2)r^2].$$

The spin dependence of the residual interaction can be studied with the $|h_{9/2}\otimes f_{7/2}\rangle$ and $|h_{9/2}\otimes f_{5/2}\rangle$ configurations. These two configurations differ by a spin flip, i.e. $|h_{9/2}\otimes f_{7/2}\rangle$ has $j_1 = l_1 - \frac{1}{2}$, $j_2 = l_2 + \frac{1}{2}$, and $|h_{9/2}\otimes f_{5/2}\rangle$ has $j_1 = l_1 - \frac{1}{2}$, $j_2 = l_2 - \frac{1}{2}$. This spin flip changes the most attractive matrix elements from the high J state ($J=8$) to the low J state ($J=2$). V_I reproduces well these features through its short-range attractive part.

The matrix elements of the empirical interaction V_{ST} obtained by Schiffer and True[2] are shown in Fig. 8. The trends of the experimental matrix elements are well reproduced and for the $|h_{9/2}\otimes h_{9/2}\rangle$, $|h_{9/2}\otimes f_{7/2}\rangle$, and $|h_{9/2}\otimes i_{13/2}\rangle$ multiplets, the standard deviation of V_{ST} is 64 keV, compared to 59 keV for V_I. V_{ST} contains seven parameters for $T=1$ states. Similar to V_I, V_{ST} for $T=1$ states con-

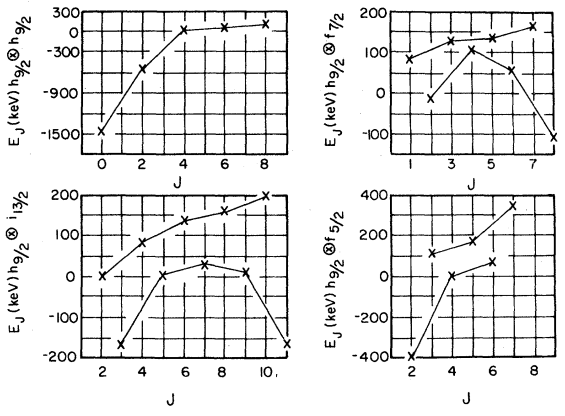

FIG. 6. Experimental diagonal $T=1$ matrix elements extracted from the ^{210}Po spectrum. The lines simply connect the data points. The odd and even J's are treated separately because of their different behavior for a short-range interaction. In each of the $|h_{9/2}\otimes f_{7/2}\rangle$, $|h_{9/2}\otimes i_{13/2}\rangle$, and $|h_{9/2}\otimes f_{5/2}\rangle$ multiplets, at most two matrix elements are attractive.

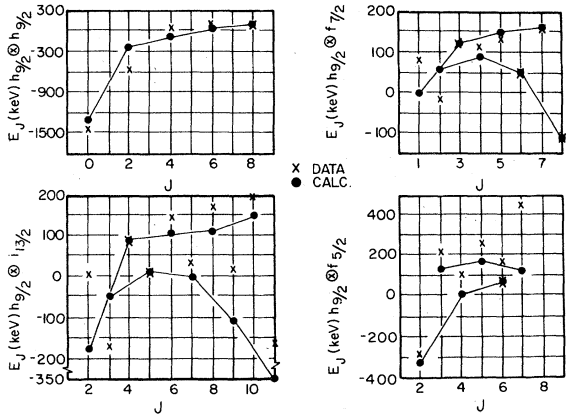

FIG. 7. Calculated $T=1$ matrix elements for the interaction V_I(●) and the experimental matrix elements (X). This interaction reproduces well the trend of the data and has a standard deviation of 80 keV.

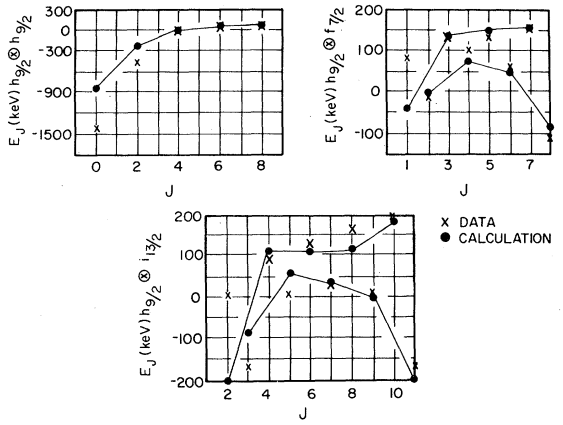

FIG. 8. Calculated $T=1$ matrix elements for the empirical Schiffer-True interaction (●) and the experimental matrix elements (X). This interaction reproduces well the trend of the data and has about the same standard deviation as the interaction V_I.

tains a short-range attractive part and a long-range repulsive part.

The matrix elements obtained from the realistic calculation of Kuo and Herling[3] for ^{210}Po are shown in Figs. 9(a) and 9(b). Figure 9(a) displays the matrix elements obtained from the bare G matrix. The experimental trends are not well reproduced. The standard deviation is 207 keV. Figure 9(b) displays the matrix elements obtained by adding the second order bubble diagram to the bare G matrix. This second order contribution improves the fit to the trend of the data and reduces the standard deviation to 100 keV. However, inclusion of the second order still does not reproduce the trend of the data as well as do the empirical matrix elements. This suggests that core polarization contributions are important and need to be calculated more accurately to improve the fit to the experimental matrix elements.

CONCLUSION

The trend of the experimentally determined matrix elements is well reproduced by the simple empirical interaction V_I. The J dependence of the matrix elements is reproduced by a short-range attractive potential while a long-range repulsive part is required to make the matrix elements slightly positive (repulsive).

A comparison of the bare Kuo-Herling G matrix elements with the experimental matrix elements shows that a large contribution from core polarization is present. The second order term improves the fit but does not reproduce the trend of the experimental matrix elements as well as the empirical interactions.

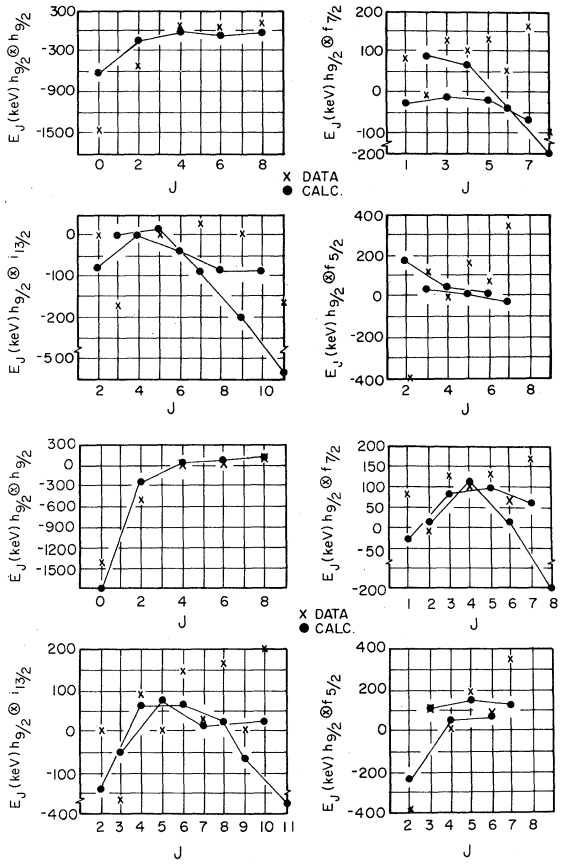

FIG. 9. (a) $T=1$ matrix elements of the bare G matrix obtained from a realistic calculation done by Kuo and Herling (Ref. 3) (●) and the experimental matrix elements (X). (b) $T=1$ matrix elements including the bare G matrix and the second order contribution from the bubble graphs, as calculated by Kuo and Herling (Ref. 3) (●) and the experimental matrix elements (X).

ACKNOWLEDGMENTS

One of the authors (R.G.) would like to thank Dr. J. Petersen from Yale University for his help with the data transfer from the Princeton to the Yale data analysis facility. We also wish to thank D. Muller, F. Calaprice, and W.H. Moore for help in obtaining these data. One of us (W.A.L.) thanks the Alfred P. Sloan Foundation for support. This research was supported in part by D.O.E. under Contract No. EY-76-C-02-3074 at Yale University and, at Princeton University, by the N.S.F. under Contract No. PNY 76-82335.

APPENDIX A

From Fig. 4(b), the $|h_{9/2}\otimes f_{5/2}\rangle$ multiplet appears to be mixed with $l=1$ states. The assignment of angular momentum based solely on the spectro-

TABLE VII. Configuration mixing between the $|h_{9/2}\otimes f_{5/2}\rangle$, $|h_{9/2}\otimes p_{3/2}\rangle$, $|h_{9/2}\otimes p_{1/2}\rangle$, and $|i_{13/2}\otimes i_{13/2}\rangle$ configurations as calculated by Kuo and Herling (Ref. 3).

Main configuration	J^π	Admixing probability	Admixed configuration	Admixing probability
$\|h_{9/2}\otimes f_{5/2}\rangle$	2^+	0.63	$\|i_{13/2}\otimes i_{13/2}\rangle$	0.20
			$\|f_{7/2}\otimes f_{7/2}\rangle$	0.12
	3^+	0.99		
	4^+	0.75	$\|i_{13/2}\otimes i_{13/2}\rangle$	0.15
			$\|h_{9/2}\otimes p_{3/2}\rangle$	0.04
	5^+	1.00		
	6^+	0.69	$\|i_{13/2}\otimes i_{13/2}\rangle$	0.07
			$\|h_{9/2}\otimes p_{3/2}\rangle$	0.20
	7^+	1.00		
$\|h_{9/2}\otimes p_{3/2}\rangle$	3^+	0.99		
	4^+	0.38	$\|i_{13/2}\otimes i_{13/2}\rangle$	0.36
			$\|h_{9/2}\otimes f_{5/2}\rangle$	0.22
	5^+	1.00		
	6^+	0.58	$\|i_{13/2}\otimes i_{13/2}\rangle$	0.07
			$\|h_{9/2}\otimes f_{5/2}\rangle$	0.30
$\|h_{9/2}\otimes p_{1/2}\rangle$	4^+	0.96		
	5^+	1.00		
$\|i_{13/2}\otimes i_{13/2}\rangle$	4^+	0.41	$\|h_{9/2}\otimes p_{3/2}\rangle$	0.56
	6^+	0.71	$\|h_{9/2}\otimes p_{3/2}\rangle$	0.20

scopic strengths is ambiguous. The spins suggested in Table I were obtained by qualitatively comparing a calculation that reproduces the $|h_{9/2}\otimes f_{7/2}\rangle$ and $|h_{9/2}\otimes i_{13/2}\rangle$ multiplets to the data.

The qualitative features predicted by V_I and the realistic calculation of Kuo and Herling are the same. Table VII shows the configuration mixing predicted by Kuo and Herling, where the model space includes all the possible two valence protons states in this major shell. The calculation shows a strong admixture between the even J states of the $|h_{9/2}\otimes f_{5/2}\rangle$, $|h_{9/2}\otimes p_{3/2}\rangle$, and $|i_{13/2}\otimes i_{13/2}\rangle$ multiplets, while the odd J states stay relatively pure.

To suggest the spins of Table I, we assumed the 3^+, 5^+, and 7^+ states of the $|h_{9/2}\otimes f_{5/2}\rangle$ multiplet to be pure. The dipole sum rule thus leads to the two possible spin assignments given in Table VIII. For both the 4^+ and 6^+ states, assignment (a) would give matrix elements with a standard deviation of order 200 keV from the predictions of the empirical interaction V_I and the realistic calculation of Kuo and Herling. However, assignment (b) gives better agreement with the sum rule and with the calculated matrix elements. Assignment (b), as given in Table I, is therefore preferred since it combines both simplicity and qualitative agreement with the calculation.

TABLE VIII. Possible spin assignments for the $|h_{9/2}\otimes f_{5/2}\rangle$ multiplet on account of the dipole sum rule.

Peak no.	(a)	(b)
16	2^+	2^+
17	6^+	4^+
18	6^+	6^+
19	3^+	3^+
20	5^+	5^+
21	4^+	6^+
22	$7^+,4^+$	$7^+,4^+$

The transition corresponding to peak 23 at 4.591 MeV is a pure $l=1$ transfer. If we assume the odd J 3^+ and 5^+ states of $|h_{9/2}\otimes p_{3/2}\rangle$ multiplet are not mixed, the level at 4.591 MeV has a spectroscopic strength consistent with the 3^+ assignment. The level at 4.624 MeV has a spectroscopic strength about 30% larger than the theoretical strength for the 5^+ state. This could be caused by the uncertainty from peak fitting. This level lies within 50 kev of the 5^+ state predicted by the empirical interaction V_I. Hence, we suggest the configuration $|h_{9/2}\otimes p_{3/2}\rangle_{5^+}$ for the level at 4.624 MeV. The other $l=1$ peaks seen in the (^{3}He,d) spectrum have small spectroscopic strengths and no spins are suggested for these levels in Table I.

APPENDIX B

Using the gyromagnetic moments μ deduced from the single-valence-nucleon nuclei around ^{208}Pb, simple rules of vector addition can be used to predict the magnetic moments of many-valence-nucleon nuclei in the ^{208}Pb region. This calculation assumes that the valence nucleons keep the

TABLE IX. Magnetic moments of nuclei in the ^{208}Pb region.

Isotope	J^π	Exc. energy (MeV)	Configuration	Mag. moments (μ_N) Experimental		Calculated
^{209}Bi [a]	$\frac{9}{2}^-$	0.000	$\pi h_{9/2}$	+4.110 6	± 0.000 2	
^{207}Pb [a]	$\frac{1}{2}^-$	0.000	$\nu p_{1/2}^{-1}$	+0.587	± 0.007	
^{205}Pb [a]	$\frac{13}{2}^-$	1.014	$\nu i_{13/2}^{-1}$	−0.975	± 0.040	
^{210}Po	6^+	1.473	$(\pi h_{9/2})^2$	+5.48	± 0.05	5.46
	8^+	1.557	$(\pi h_{9/2})^2$	+7.35	± 0.05	7.28
^{211}At	$\frac{21}{2}^-$	1.417	$(\pi h_{9/2})^3$	+9.54	± 0.10	9.55
	$\frac{29}{2}^-$	2.641	$(\pi h_{9/2})^3$	+15.31	± 0.13	
^{209}At	$\frac{21}{2}^-$	1.428	$(\pi h_{9/2})^3$	+9.98	± 0.21	9.55
	$\frac{29}{2}^-$	2.429	$(\pi h_{9/2})^3$	15.37	± 0.29	
^{212}Rn	8^+	1.671	$(\pi h_{9/2})^4$	+7.29	± 0.10	7.28
^{213}Fr	$\frac{21}{2}^-$	1.590	$(\pi h_{9/2})^5$	9.320	± 0.037	9.55
	$\frac{29}{2}^-$	2.536	$(\pi h_{9/2})^5$	15.08	± 0.29	
^{214}Ra	8^+	1.865	$(\pi h_{9/2})^6$	7.120	± 0.032	7.28
^{208}Po	8^+	1.533	$(\pi h_{9/2})^2$	+7.288	± 0.088	7.28
^{206}Po	8^+	<1.582	$(\pi h_{9/2})^2$	+7.35	± 0.10	7.28
^{204}Po	8^+	<1.704	$(\pi h_{9/2})^2$	+7.38	± 0.10	7.28
^{202}Po	8^+	<1.730	$(\pi h_{9/2})^2$	7.45	± 0.12	7.28
^{205}Tl	$\frac{1}{2}^+$	0.000	$(\pi s_{1/2}^{-1})$	+1.638 213 4	± 0.000 000 7	
^{203}Tl	$\frac{1}{2}^+$	0.000	$(\pi s_{1/2}^{-1})$	+1.622 257	± 0.000 001	
^{201}Tl	$\frac{1}{2}^+$	0.000	$(\pi s_{1/2}^{-1})$	+1.61	± 0.02	
^{199}Tl	$\frac{1}{2}^+$	0.000	$(\pi s_{1/2}^{-1})$	+1.60	± 0.02	
^{197}Tl	$\frac{1}{2}^+$	0.000	$(\pi s_{1/2}^{-1})$	+1.58	± 0.02	
^{195}Tl	$\frac{1}{2}^+$	0.000	$(\pi s_{1/2}^{-1})$	+1.58	± 0.04	
^{208}Bi	10^-	1.571	$\nu i_{13/2}^{-1} \otimes \pi h_{9/2}$	2.633	± 0.013	
^{206}Bi	10^-	1.044	$\nu i_{13/2}^{-1} \otimes \pi h_{9/2}$	2.631	± 0.024	2.67
^{206}Pb	7^-	2.200	$\nu p_{1/2}^{-1} \otimes \nu i_{13/2}$	−0.151 9	± 0.002 8	−0.37
^{206}Pb	6^-	2.384	$\nu p_{1/2}^{-1} \otimes \nu i_{13/2}^{-1}$	+0.78	± 0.42	−1.47

[a] Magnetic moments used as input to the calculations. The data are from Ref. 17.

same gyromagnetic moments μ independent of the presence of other valence nucleons. The calculation is compared to the experimental moments in Table IX. As shown, except for two moments in ^{206}Pb, the calculation agrees with the experimental moments well. Table IX also shows the experimental moments of a series of isotopes of Po and Tl having an even number of neutrons. The moments stay remarkably constant. These comparisions suggest the independence of the core polarization induced by a valence nucleon in the presence of other valence nucleons.

*Present address: Dept. of Physics, S.U.N.Y. at Albany, Albany, New York 12222.

[1] R. K. Bansal and J. B. French, Phys. Lett. 19, 223 (1965); J. B. French in *Proceedings of the International School of Physics "Enrico Fermi", Course XXXVI, 1966*, edited by C. Bloch (Academic, New York, 1966).

[2] J. P. Schiffer and W. W. True, Rev. Mod. Phys. 48,

191 (1976).
[3]T. T. S. Kuo and G. H. Herling, NRL Memorandum Report No. 2258, Naval Research Laboratory, unpublished.
[4]W. A. Lanford, W. P. Alford, and H. W. Fulbright, Report No. UR-NSRL-44, University of Rochester (unpublished).
[5]P. D.Kunz (unpublished).
[6]J. S. Lilley and N. Stein, Phys. Rev. Lett. 19, 709 (1967); 19, 1000 (1967).
[7]B. H. Wildenthal, B. M. Preedom, E. Newman, and M. R. Cates, Phys. Rev. Lett. 19, 960 (1967).
[8]A. Bohr and B. R. Mottelson, *Nuclear Structure* (Benjamin, Reading, Mass., 1969), Vol. I.
[9]R. Groleau, Ph.D. thesis, Yale University, 1980 (unpublished).
[10]J. B. McGrory and T. T. S. Kuo, Nucl. Phys. A247, 283 (1975).
[11]M. H. MacFarlane and J. B. French, Rev. Mod. Phys. 32, 567 (1960).
[12]B. L. Cohen, in *Nuclear Spin-Parity Assignments*, edited by N. B. Gove and R. L. Robinson (Academic, New York, 1966).
[13]L. J. Jardine, S. G. Prussin, and J. M. Hollander, Nucl. Phys. A190, 261 (1972).
[14]I. Hamamoto, Phys. Rep. 10C, 2 (1974).
[15]C. Ellegaard, P. D. Barnes, R. Eisenstein, E. Romberg, T. S. Bhotia, and T. R. Canada, Nucl. Phys. A206, 83 (1973).
[16]J. Bardwick and R. Tickle, Phys. Rev. 171, 1305 (1968).
[17]*Table of Isotopes*, 7th ed., edited by C. M. Lederer and V. S. Shirley (Wiley, New York, 1970).